

Spring Phytoplankton Distributions and Primary Productivity in Waters off Northern Norway

Smith, Jr. Walker O.¹, Meng Rui², and Basedow S L³

¹VIMS, William & Mary; School of Oceanography, Shanghai Jiao Tong University

²Shanghai Jiao Tong University

³UiT

November 16, 2022

Abstract

* Phytoplankton distributions and primary productivity were assessed off the northern coast of Norway in spring. Biomass and productivity were greatest off the continental shelf during the period of observations. * A satellite climatology showed that blooms usually form on the continental shelf first, and spread to deeper waters from 2-4 weeks after the shelf bloom. * The *Calanus finmarchicus* population had the potential for removing substantial amounts of chlorophyll each day, but phytoplankton vertical distributions were controlled by passive sinking.

Hosted file

agusupporting-information_8_15.docx available at <https://authorea.com/users/524181/articles/595410-spring-phytoplankton-distributions-and-primary-productivity-in-waters-off-northern-norway>

1 **Spring Phytoplankton Distributions and Primary Productivity in Waters off**
2 **Northern Norway**

3
4 **R. Meng¹, W.O. Smith, Jr.^{1,2}, and S. L. Basedow³**

5 ¹ School of Oceanography, Shanghai Jiao Tong University, Shanghai, China

6 ² Virginia Institute of Marine Science, William & Mary, Gloucester Pt., VA, USA

7 ³ UiT, The Arctic University of Norway, Tromsø, Norway

8
9 Corresponding author: Walker O. Smith, Jr. (wos@vims.edu); ORCID Number

10 **0000-0003-4304-1980**

11
12 ORCID Numbers: R. Meng 0000-0003-1947-2975

13 S. Basedow 0000-0001-6000-6090

14
15 **Key Points:**

- 16 • Phytoplankton distributions and primary productivity were assessed off the northern coast
17 of Norway in spring. Biomass and productivity were greatest off the continental shelf
18 during the period of observations.
- 19 • A satellite climatology showed that blooms usually form on the continental shelf first,
20 and spread to deeper waters from 2-4 weeks after the shelf bloom.
- 21 • The *Calanus finmarchicus* population had the potential for removing substantial amounts
22 of chlorophyll each day, but phytoplankton vertical distributions were controlled by
23 passive sinking.

24
25 **Key Words:** phytoplankton, Norway, *Calanus finmarchicus*, primary productivity, chlorophyll

26 **Abstract**

27 The distribution of phytoplankton, zooplankton and hydrographic features off the coast of
28 northern Norway were assessed in late April – early May, 2019 using ship-based observations
29 (CTD casts and Moving Vessel Profilers) and autonomous vehicles. A satellite chlorophyll
30 climatology allowed us to place our in situ observations within a longer temporal sequence.
31 Substantial spatial and temporal variability was observed in both the observations and climatology.
32 Phytoplankton accumulation usually is initiated in the south on the continental shelf, and advanced
33 in a northerly direction through time. Accumulations in the surface layer of deeper waters off the
34 continental shelf occurred 2-3 weeks later than those on the shelf. During our survey primary
35 productivity was greatest in offshore waters where nutrients were not depleted and exceeded 2 g
36 $\text{C m}^{-2} \text{ d}^{-1}$. The greatest *Calanus finmarchicus* abundances were associated with low chlorophyll
37 concentrations, but estimates of phytoplankton growth and zooplankton removal suggested that
38 *Calanus* was responsible for only a minor portion of the observed chlorophyll changes. Vertical
39 changes in chlorophyll were related to passive sinking rather than grazing. Understanding the
40 spatial and temporal variations of the coupling of phytoplankton to zooplankton is essential to
41 effective management of the important commercial species of the region.

42

43

44 **Plain Language Summary**

45 Coastal waters of Norway are sites for harvests of a number of commercially important species,
46 including cod and *Calanus finmarchicus*, a copepod ~ 3 mm in length, that is a key species in the
47 marine food web. We studied the distribution of phytoplankton, the food for *Calanus*, in the
48 waters off northern Norway in late April – early May in 2018. We also generated a seasonal
49 average of chlorophyll to place our observations within a broader context. Accumulations of
50 phytoplankton begin in more southern waters of the shallow continental shelf and advanced along
51 the coast to the north. Simultaneously, phytoplankton growth and accumulation in deeper waters
52 off the continental shelf begins about 2-3 weeks after that in shallow waters, which is less of a
53 delay than previously thought. Copepods generally were related to low chlorophyll concentrations,
54 but had the potential for removing a substantial amount of phytoplankton daily. However,
55 comparing potential phytoplankton growth and removal by *Calanus* suggested that the copepod
56 had a minor role in regulating phytoplankton biomass during the period of our observations.
57 Passive sinking of phytoplankton appeared to be important in regulating vertical structure.
58 Understanding the variability in space and time that occurs naturally in coastal Norwegian waters
59 will greatly assist the management of the harvest of critically important species.

60

61 **1 Introduction**

62 Waters off the Norwegian Coast have received considerable attention due to the large
63 populations of commercially valuable species [e.g., Northeast Arctic cod (*Gardus morhua*), the
64 copepod *Calanus finmarchicus*, and Norwegian spring spawning herring (*Clupea harengus*)] that
65 have supported local and regional fisheries for centuries. Understanding the distribution of these
66 species, and the food web that supports them, is critical to an effective management strategy.
67 Phytoplankton distributions in the region have also been studied intensively, given that
68 phytoplankton support the food web in which *C. finmarchicus* serves as the dominant grazer and
69 food for higher trophic species (as well as being commercially harvested). In general, coastal
70 waters support a spring bloom that reaches its maximum in late April, while chlorophyll
71 concentrations in off-shore waters have been suggested to become maximal about one month later
72 (Bagøien et al., 2012). Substantial spatial and temporal variations occur among years, as winds,
73 fresh water inputs from fjords, storms, and bathymetry all influence local growth and distributions
74 of phytoplankton.

75 Phytoplankton biomass is often assessed by measuring chlorophyll concentrations. Methods to
76 measure chlorophyll are well standardized; furthermore, as fluorescence is also a routine parameter
77 on a variety of platforms, those values can be calibrated against discrete chlorophyll measurements
78 and converted into chlorophyll concentrations. Examples of platforms which routinely measure
79 fluorescence on small vertical and horizontal scales are CTDs, autonomous vehicles (such as
80 gliders and wave gliders), and moving vessel profilers. The different sampling technologies allow

81 for a greater spatial and temporal resolution of phytoplankton biomass and provide new insights
82 into the processes controlling phytoplankton growth and accumulation (Madhavan et al., 2012;
83 Kaufman et al., 2014; Ryan-Keogh & Smith, 2021).

84 Carbon fixation by phytoplankton during photosynthesis has traditionally been measured using
85 radiotracer techniques (e.g., Steemann Nielsen, 1952; Marra, 2009; Marra et al., 2021), in which
86 samples are collected from known isolumens, ^{14}C -bicarbonate added, and incorporation quantified
87 after samples are incubated in a known irradiance environment on the deck of a ship. These
88 measurements are an important system variable, in that it describes the rate of growth of
89 phytoplankton and puts an upper limit on energy available within the food web. However,
90 considerable limitations and uncertainties remain in assessing and comparing isotopic
91 measurements. For example, collecting seawater and placing the samples in bottles removes
92 phytoplankton from their natural, turbulent environment and can induce serious bottle effects due
93 to the death of microzooplankton grazers (Eppley, 1982). The size of bottles also precludes the
94 inclusion of macrozooplanktonic grazers such as copepods, thus altering rates of nutrient cycling.
95 The time of the incubation start also influences net fixation, as does the length of incubation
96 (Marra, 2009), and vertical temperature variations and their impacts on photosynthesis are usually
97 not considered or controlled (Ma & Smith, 2022). As a result, it is difficult to unambiguously
98 assign the measured isotopic rate as being a measure of net or gross photosynthesis; such
99 measurements clearly cannot be completed on the same space and time scales that are sampled by
100 platforms measuring fluorescence, oxygen, temperature and salinity.

101 An alternative method has been introduced that uses oceanographic data to estimate primary
102 productivity: a vertically-resolved productivity model (Behrenfeld & Falkowski, 1997a,b;
103 Friedrichs et al., 2009; Lee et al., 2015). This procedure has been applied to satellite data, as the
104 model inputs are sea surface temperature, irradiance, and surface chlorophyll concentrations, all
105 parameters that can be measured remotely. The model can also be applied within the water column
106 to estimate vertically resolved productivity using the same parameters along with an assumed
107 photosynthetic response (Ma & Smith, 2022). As these variables are routinely collected using
108 CTDs, gliders and profilers, estimates of primary production on small vertical and horizontal scales
109 can be made during surveys of specific areas and provide insights into the variability of
110 productivity on the same scales as biomass.

111 In April-May, 2019 we conducted a cruise off the Lofoten coast to assess the distribution of
112 phytoplankton, the physical processes occurring on the continental shelf, shelf-break and slope,
113 and their impacts on the copepod *Calanus finmarchicus*. *C. finmarchicus* is a critically important
114 species in the region, as it is the keystone species of the regional food web and is also commercially
115 harvested as a result of the massive aggregations that occur (Basedow et al., 2019). These
116 aggregations can be observed from space due to the animal's pigments, further emphasizing the
117 importance of this species to the region (Basedow et al., 2019; Dong et al., 2021). Understanding
118 the relationship of both physical factors and phytoplankton distributions is important to managing
119 this resource. Given its substantial abundance, we hypothesized that *Calanus* grazing would be
120 the dominant phytoplankton loss process. The objective of our survey was to investigate how

121 physical, biogeochemical and biological processes are coupled on the Norwegian shelf-slope
122 system. We also placed our results within a climatology of the region to determine the stage of
123 bloom development in the shelf-slope area. Primary productivity was estimated by two different
124 models to constrain the turnover of phytoplankton and to provide a means to estimate the impact
125 of grazing by zooplankton. We focused on the relationships among hydrography, phytoplankton
126 and zooplankton distributions and their variability in space and time.

127

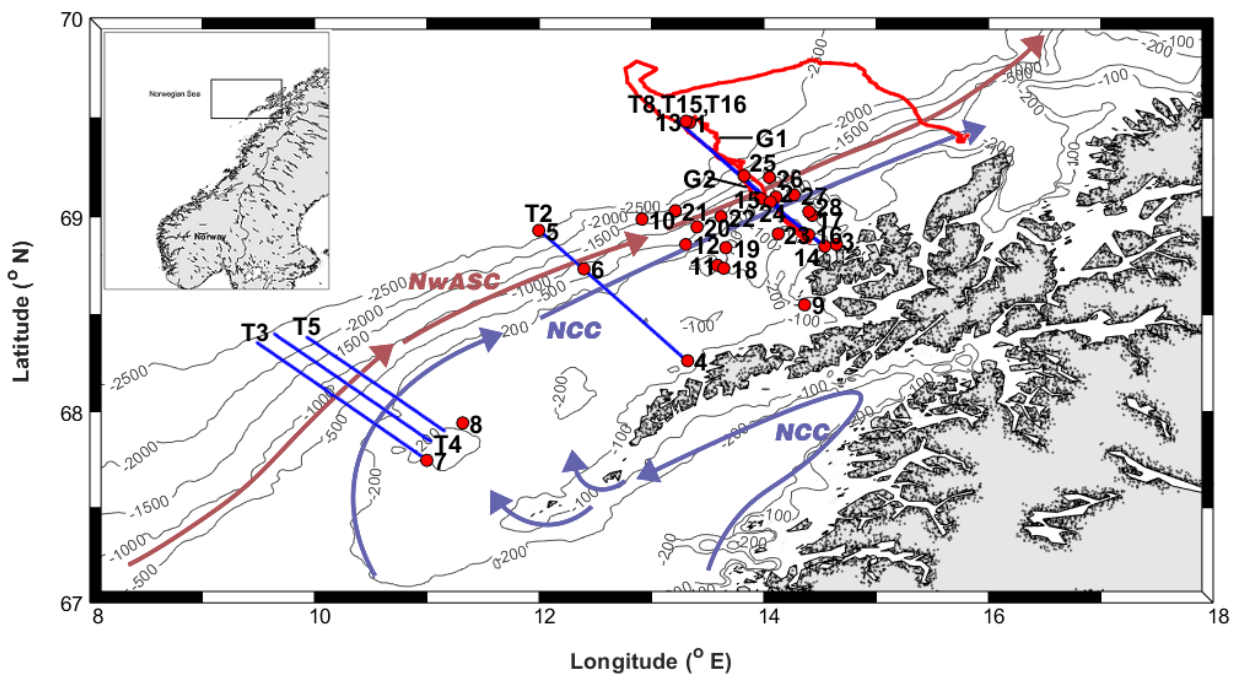
128 **2 Materials and Methods**

129 2.1 Study region

130 The study site was the continental shelf and shelf slope area between 67.7 to 69.7°N and 9.5
131 to 15.8°E off northern Norway (Figure 1). The main currents in this area are the Norwegian Coastal
132 Current (NCC) and Norwegian Atlantic Slope Current (NwASC; Dong et al., 2021). NCC is a
133 buoyancy-driven, northward flowing current trapped near the Norwegian coast. It originates at the
134 Baltic entrance to the Skagerrak and receives coastal freshwater inputs as it flows north (Skagseth
135 et al., 2011). The NwASC carries warm, saline, nutrient-rich water along the Norwegian
136 continental shelf break. The NCC and NwASC carry cold and fresh Norwegian Coastal Water
137 (NCW, $S < 34.5$) and warm and more saline North Atlantic Water (NAW, $S > 35$) along the
138 Norwegian continental shelf, respectively (Mork et al., 1981; Pedersen et al., 2005). A salinity
139 front forms between the two water masses and is usually located near the shelf break, delineated
140 by the 34.8 isohaline (Sætre, 1999).

141 2.2 Sample collection

142 Data were collected during spring, 2019 (April 27 – May 12) from the *R.V. Helmer Hanssen*
143 near the Lofoten-Vesterålen Islands as part of the STRESSOR program (Collaborative Studies of
144 Two Resource Ecosystems in Shelf, Slope and Oceanic Regions of the Norwegian and South-
145 China Seas; Figure 1). Surface photosynthetically active radiation (PAR) was measured
146 continuously using an on-deck Biospherical/Licor 4Π sensor. Water samples were obtained at 28
147 stations (Figure 1) using a SeaBird 911+ CTD-rosette system equipped with Niskin bottles and an
148 in situ PAR sensor. A total of 17 Moving Vessel Profiler (MVP; Rolls Royce Canada, Ltd.)



149 **Figure 1.** Map showing the CTD station locations and the transects occupied by the moving
150 vessel profiler (blue) and the glider (red). Approximate location of currents [the Norwegian
151 Coastal Current (NCC) in blue and the Norwegian Atlantic Slope Current (NwASC) in red] are
152 also shown. The inset shows the location of the study off the coast of Norway.

153
154

155 transects were completed across continental shelf and slope; seven were used in this analysis.
156 Finally, a glider (Seaglider, Kongsberg) equipped with a WetLabs ECO puck to collect
157 fluorescence and optical backscatter data sampled in transects roughly perpendicular to the shelf
158 (Figure 1). Dates and locations (start and end) of all analyzed transects are listed in Supplemental
159 Table S1. Unfortunately, no CTD casts were taken in close proximity to the glider, so the glider
160 fluorescence data could not be reliably converted to chlorophyll units and are reported in arbitrary
161 units.

162 2.3 CTD sampling

163 A SeaBird 911+ CTD was deployed on a rosette from the surface to the bottom at shallow
164 stations, or through 600 m at deeper stations. All sensors were calibrated prior to the cruise. Water
165 samples for nutrients, chlorophyll, particulate organic carbon and nitrogen, and biogenic silica
166 were collected from 5-L Niskin bottles mounted on the rosette frame. Nutrient samples (50 mL) at
167 selected depths (0, 5, 10, 20, 50 m and bottom) were collected in centrifuge tubes (tubes were
168 rinsed with seawater three times before samples were collected), and frozen upright at -20°C.
169 Nutrient concentrations (nitrate, nitrite, phosphate, silicate) were analyzed using automated
170 techniques at University of Tromsø using a QuAAtro39 Seal autoanalyzer.

171 Chlorophyll, particulate organic carbon and nitrogen, and biogenic silica were collected in
172 opaque, acid-cleaned bottles. Chlorophyll samples (generally 250 mL) were filtered through
173 Whatman GF/F filters under low vacuum ($<1/2$ atm) and the filters immediately frozen for later
174 analyses. In the laboratory samples were extracted in methanol and analyzed fluorometrically on

175 a Turner Designs fluorometer calibrated with commercially purified chlorophyll *a*. Particulate
176 organic carbon/nitrogen samples were filtered through combusted (450°C for 4 h) 25 mm GF/F
177 filters under low pressure, rinsed with ca. 5 mL 0.01 N HCl in filtered seawater, placed in
178 combusted glass vials, covered with combusted aluminum foil, and dried at 60°C for later analyses
179 (Gardner et al., 2000). Blanks were filters that had a few mL of seawater filtered through them and
180 processed identically. All samples were analyzed on a Unicube Elementar elemental analyzer
181 using sulfanilamide as a standard. Biogenic silica samples were filtered through 0.6 µm
182 polycarbonate filters (Whatman), folded, placed in glassine envelopes, dried at 60°C and returned
183 to the laboratory for analyses. Filters were digested in NaF and the resultant silicic acid measured
184 spectrophotometrically (Brzezinski & Nelson, 1989).

185 CTD fluorescence data were calibrated by correlating discrete sample chlorophyll
186 concentrations collected at known depths with fluorescence values at the same depths (n=189).
187 The resulting significant regression [$\text{Chl (mg m}^{-3}\text{)} = 0.56 \times \text{Fl} - 0.25$; $R^2 = 0.89$] was applied to all
188 fluorescence data, providing a detailed vertical description (1-m resolution) of phytoplankton
189 biomass.

190 2.4 MVP sampling

191 High resolution cross-shelf transects were obtained using a moving vessel profiler fitted with
192 a Seabird CTD (sampling rate of 25 Hz), a fluorescence sensor and LOPC (Laser Optical Plankton
193 Counter; sampling rate 2 Hz) to obtain information on hydrological and particle properties. The
194 MVP was towed behind the ship as it steamed 6-7 kts, continuously taking nearly vertical profiles

195 in the upper 600 m before returning to the surface. The MVP transects ranged between 80 to 90
196 km long and sampled the shelf, slope, and deep water (Figure 1). All transects were completed
197 during darkness. MVP fluorescence data were calibrated in a manner similar to those from the
198 CTD casts. Discrete chlorophyll samples ($n = 45$) were collected at the surface from the ship's
199 flowing seawater system (which had been cleaned prior to the cruise) when the MVP reached the
200 surface. The resulting significant regression between chlorophyll and fluorescence [$\text{Chl} (\text{mg m}^{-3})$
201 $= 97.2 \times \text{Fl} + 12.8; R^2 = 0.85$] was applied to all MVP data collected during the cruise. CTD data
202 were recorded with a high frequency (25 Hz), and were then converted to the frequency of the
203 LOPC data (2 Hz).

204 The LOPC provides high spatial resolution measurements of particle sizes. It measures the
205 numbers and equivalent spherical diameter (ESD) of particles between 100 μm and ca. 3 cm
206 (Herman et al., 2004), and additional features for particles $>$ ca. 800 μm ESD, but does not provide
207 taxonomic data or information on the activity of the particles. However, previous investigations in
208 this region have shown there are relatively few zooplankton species; furthermore, the LOPC has
209 been shown to provide reliable *Calanus finmarchicus* copepodite abundance estimates (Basedow
210 et al., 2008; Gaardsted et al., 2010). LOPC ESD data ranging between 1.0 and 2.0 mm were
211 selected as an estimate of *C. finmarchicus* adult and stage V copepodite abundance (Basedow et
212 al., 2013). In addition, an attenuation index ($\text{AI} \geq 0.4$) was applied when computing *C.*
213 *finmarchicus* abundance from MEPs (multi-element particle) data to exclude transparent MEPs
214 such as marine snow (Basedow et al., 2013). Zooplankton concentrations were estimated by

215 normalizing LOPC counts by the volume of filtered water. Data from down-profiles was used for
216 abundance calculation, as upward-profiles tend to yield less precise values for water flow through
217 the LOPC.

218 2.5 Glider sampling

219 An autonomous underwater vehicle (glider) was deployed to collect observations of ocean
220 water properties and estimates of velocity fields. The glider oscillated along transects roughly
221 perpendicular to the shelf break (Figure 1) and profiled from the surface to 1000 m (or close to the
222 bottom). Fluorescence data could not be calibrated and converted to chl *a* concentrations, as CTD
223 stations that were co-located along glider sampling path were not closely matched with glider
224 sampling in time. Therefore, fluorescence data are reported in arbitrary units and used to represent
225 the relative phytoplankton concentrations. Only data from the upper 200 m (temperature, salinity,
226 and fluorescence) were used.

227 2.6 Primary productivity estimates

228 A bio-optical model to estimate vertically resolved primary productivity was developed using
229 the temperature and chlorophyll distributions obtained from both the CTD and MVP. The model
230 was based on the formulations of Behrenfeld and Falkowski (1997a,b) where depth-resolved (at
231 1-m intervals) productivity is a function of temperature, irradiance (PAR), an assumed
232 photosynthetic response, and chlorophyll concentration (Eq. 1):

$$233 \quad PP = C_z \times P_{opt}^B \times f(E_0) \quad (\text{Eq. 1})$$

234 where PP is primary productivity ($\text{mg C m}^{-3} \text{ d}^{-1}$), C_z is chlorophyll concentration (mg chl m^{-3}) at
 235 depth z (m), P_{opt}^B the maximum photosynthetic rate within the water column ($\text{mg C (mg chl)}^{-1}$
 236 h^{-1}), and $f(E_0)$ the photon flux density at each depth that was measured directly by the CTD PAR
 237 sensor. Not all CTD casts or MVP profiles were completed during the day; therefore, direct
 238 measurements of attenuation within the water column were not always available. To generate
 239 potential irradiance attenuation profiles, the relationship between chlorophyll and attenuation
 240 (Morel, 1974; Morel et al., 1998) was used and corrected for an offset that was observed from
 241 casts conducted during the day. We believe this offset was due to dissolved organic carbon that
 242 originated from the freshwater inflows (Smith et al., 2021). A photosynthesis-irradiance response
 243 was assumed (Eq. 2):

$$P_z^B = P_{opt}^B \times \tanh \left[E_z / E_k \right] \quad (\text{Eq. 2})$$

244 (Platt & Jassby, 1976). E_k values were taken from Boumann et al. (2017), with $E_k = 0.15 \times E_0$,
 245 when E_0 (surface PAR) $< 100 \mu\text{mol photons m}^{-2} \text{ s}^{-1}$, and $E_k = 0.25 \times E_0$ when $E_0 > 100 \mu\text{mol photons}$
 246 $\text{m}^{-2} \text{ s}^{-1}$. P_{opt}^B was derived using the 7-order regression derived by Behrenfeld & Falkowski (1997b)
 247 that was based on 1,698 radioisotope profiles measured throughout the ocean. A photoinhibition
 248 term based on the same data set was also included that reduced productivity when daily irradiance
 249 was $> 3 \mu\text{mol photons m}^{-2} \text{ d}^{-1}$ (Behrenfeld & Falkowski, 1997b). E_z values were derived from the
 250 in situ PAR data collected during the CTD casts or estimated using the derived attenuation
 251 coefficients. Integrated, euphotic zone productivity was estimated by trapezoidal integrations of
 252 the 1-m estimates from the surface to the 1% isolume. Integrated daily productivity at all stations
 253

254 used the measured surface PAR data starting upon recovery of the CTD cast and continuing for 24
255 h. All integrated daily PAR data included dark periods at night.

256 A second method of estimating integrated productivity was used, based on surface temperature
257 and chlorophyll distributions (Behrenfeld & Falkowski, 1997a,b). Productivity was estimated from
258 surface chl *a* concentration, daily irradiance (PAR), day length (DL), euphotic zone depth (the
259 depth to which 1% of surface irradiance penetrates), and the optimum photosynthetic rate (P_{opt}^B)
260 of phytoplankton (Eq. 3):

$$261 \quad PP_{eu} = 0.66125 \times P_{opt}^B \times \left[\frac{E_0}{E_0 + 4.1} \right] \times Z_{eu} \times Chl\ a \times DL \quad (\text{Eq. 3})$$

262 where PP_{eu} is the integrated daily euphotic zone productivity ($\text{mg C m}^{-3} \text{ d}^{-1}$), P_{opt}^B is the
263 optimum photosynthetic rate of phytoplankton ($\text{mg C (mg Chl } a)^{-1} \text{ h}^{-1}$), E_0 is daily PAR at the
264 seawater surface ($\text{mol photons m}^{-2} \text{ d}^{-1}$), Z_{eu} is euphotic depth (m), Chl *a* is surface Chl *a*
265 concentration ($\text{mg Chl } a \text{ m}^{-3}$), and DL is the daily photoperiod (h). P_{opt}^B was estimated the
266 temperature-dependent equation from Behrenfeld and Falkowski (1997b).

267 Net seasonal production was estimated from nutrient deficits (Bates et al., 1998; Smith &
268 Asper, 1999). Deep-water concentrations were taken from Bagøien et al. (2012), who compiled
269 nutrient and mixed layer depths from coastal Norway and the Atlantic waters offshore. Winter
270 mixed-layer depths in coastal waters averaged ca. 50 m, and in Atlantic waters > 200 m. Winter
271 (before chlorophyll levels increased above 0.25 mg m^{-3}) nitrate and silicic acid concentrations in
272 coastal waters are 8 and 4 μM , respectively, and in Atlantic water 12 and 5 μM . Net seasonal
273 removal was estimated from Eq. 4:

274
$$\Delta NO_3 = \int_{50}^0 NO_3(winter) - \int_{50}^0 NO_3(obs) \quad (\text{Eq. 4})$$

275 where ΔNO_3 is the seasonal nitrate removal, $NO_3(winter)$ is the integrated (from 0 to 50 m)
276 winter mixed-layer nitrate concentration, and $NO_3(obs)$ is the measured integrated nitrate
277 concentration at each station during the period of observations. The deficits were converted to
278 carbon units using the Redfield ratio. Silicic acid reductions were also calculated from Eq. 4 to
279 estimate diatomaceous production and converting the Si removal to nitrogen and carbon units
280 using a Si/N molar ratio of 1 (Brzezinski, 1985). Growth and nutrient removal were assumed to
281 start on March 1. Daily net community production rates were estimated from the nitrate removal
282 divided by the number of days of growth. Similarly, diatom net community production was derived
283 from silicic acid removal after converting to carbon units.

284 2.7 Satellite Chlorophyll *a* data

285 To place our observations within a broader seasonal progression of phytoplankton biomass in
286 spring, satellite chlorophyll *a* data were taken from the NASA Ocean Color archive
287 (<https://oceancolor.gsfc.nasa.gov>) to generate a regional climatology. A total of 128 remote
288 sensing images from March to May in 2000-2019 using Level 2 data from the MODIS Terra and
289 Aqua satellites and the VIIRS mission (4 km resolution) were acquired and processed to generate
290 the climatology. Clouds, darkness, and angle between sunlight and satellite sensors limit ocean
291 color sensor signals in high latitude systems; given the frequent cloudy conditions found in
292 northern Norway during spring, only limited chlorophyll *a* data were available during March to
293 May. We binned chlorophyll *a* data into 10-day intervals to generate the satellite climatology.

294 2.8 Data processing

295 Mixed layer depths (MLD) were determined from CTD, MVP and glider density profiles using
296 the threshold method. MLD was defined as the depth at which seawater potential density changed
297 by 0.03 kg m^{-3} relative to the potential density at 5 m. One complete oscillation of each instrument
298 was averaged to give a profile for use in the models. Both MVP and glider data were interpolated
299 to standard depths and locations before MLD calculation. Brunt-Väisälä frequencies (N^2) were
300 determined from salinity, temperature, pressure and latitude at each CTD station by using
301 GibbsSeaWater toolbox (TEOS-10).

302 2.9 Statistical analysis

303 Linear regressions were performed by a least-square analysis, and the coefficient of
304 determination (R^2) was applied to show the percentage of the variability attributable to the
305 response. P-values were calculated using an F-test, with significance levels set a priori at 0.05. A
306 two-sample t-test was performed to examine whether the differences that occurred between the
307 two tested samples were significant. All statistical analyses were performed using MATLAB
308 version R2020b.

309

310 **3 Results**

311 3.1 Hydrography

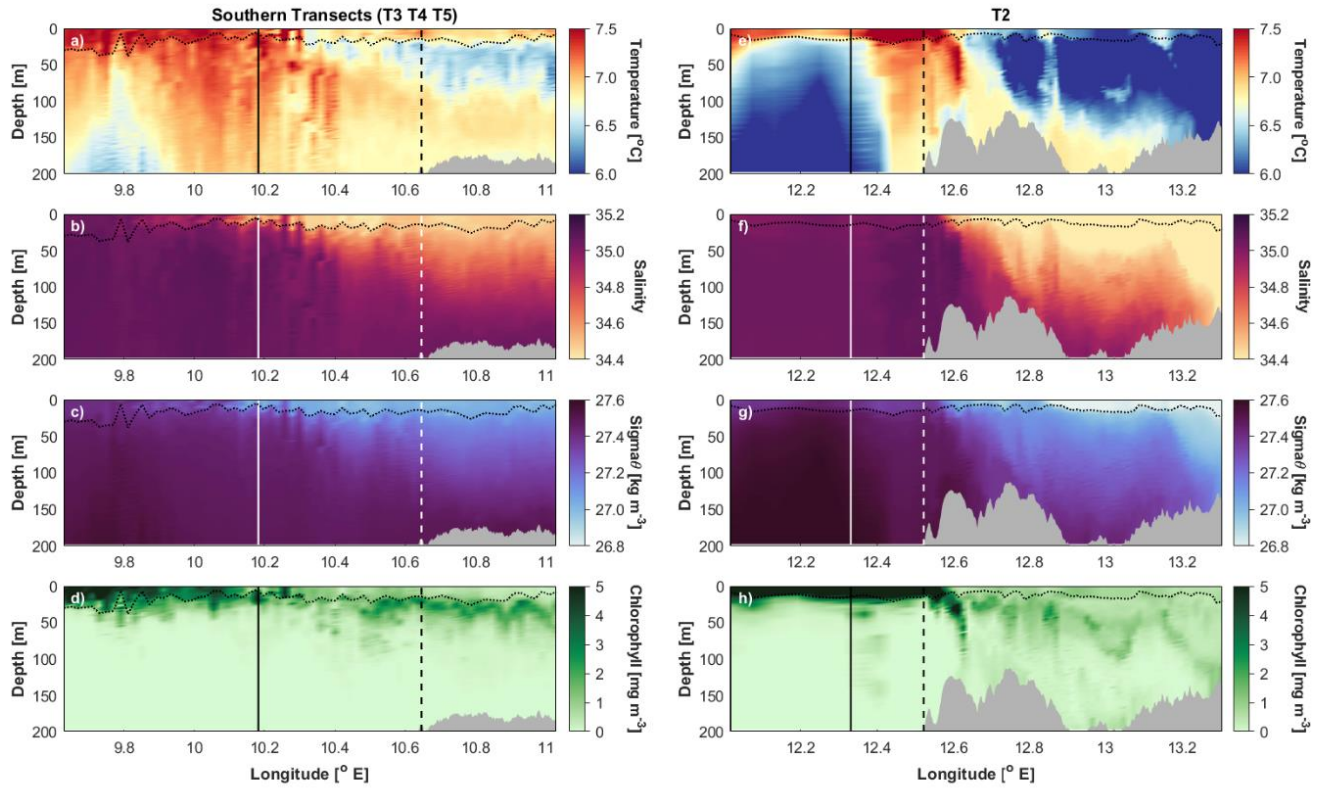
312 Sea surface temperatures (SST) ranged between 5.34 and 7.56°C , and daily surface PAR
313 ranged between 4.57 and $30.4 \text{ mol photons m}^{-2} \text{ d}^{-1}$. Colder waters ($<6.5^\circ\text{C}$) were generally confined

314 to the shelf, although they were also observed over the continental slope near the end of our cruise
315 when the front delineating Norwegian Coast Current (NCC) and Norwegian Atlantic Slope Current
316 (NwASC) broke down and shelf-slope exchanges occurred (Dong et al., 2021). Surface salinities
317 of the northern shelf stations ranged between 33.5 and 34.8, with fresher waters (<34.6) being
318 largely confined to the shelf (Figures 2,3,4). Northern slope salinities ranged between 34.1 - 35.1,
319 indicative the presence of both Norwegian Coastal Water (NCW) and North Atlantic Water
320 (NAW). Mixed layer depths were generally between 9 and 50 m (Table 1, Table S2), being shallow
321 within the southern shelf and northern shelf-break stations (13 ± 2.8 and 13 ± 6.3 m; Table 1).
322 Brunt-Väisälä frequencies fluctuated in the upper 50 m (Table S2). Higher N^2 values were found
323 in the northern shelf break and slope region, with a mean value of $8.40 \times 10^{-5} \text{ s}^{-1}$. The N^2 from the
324 northern shelf stations and stations located in the NCW were greater than the N^2 from deep-water
325 stations and those in the NAW, indicating that near-shore waters were more strongly stratified than
326 the offshore waters.

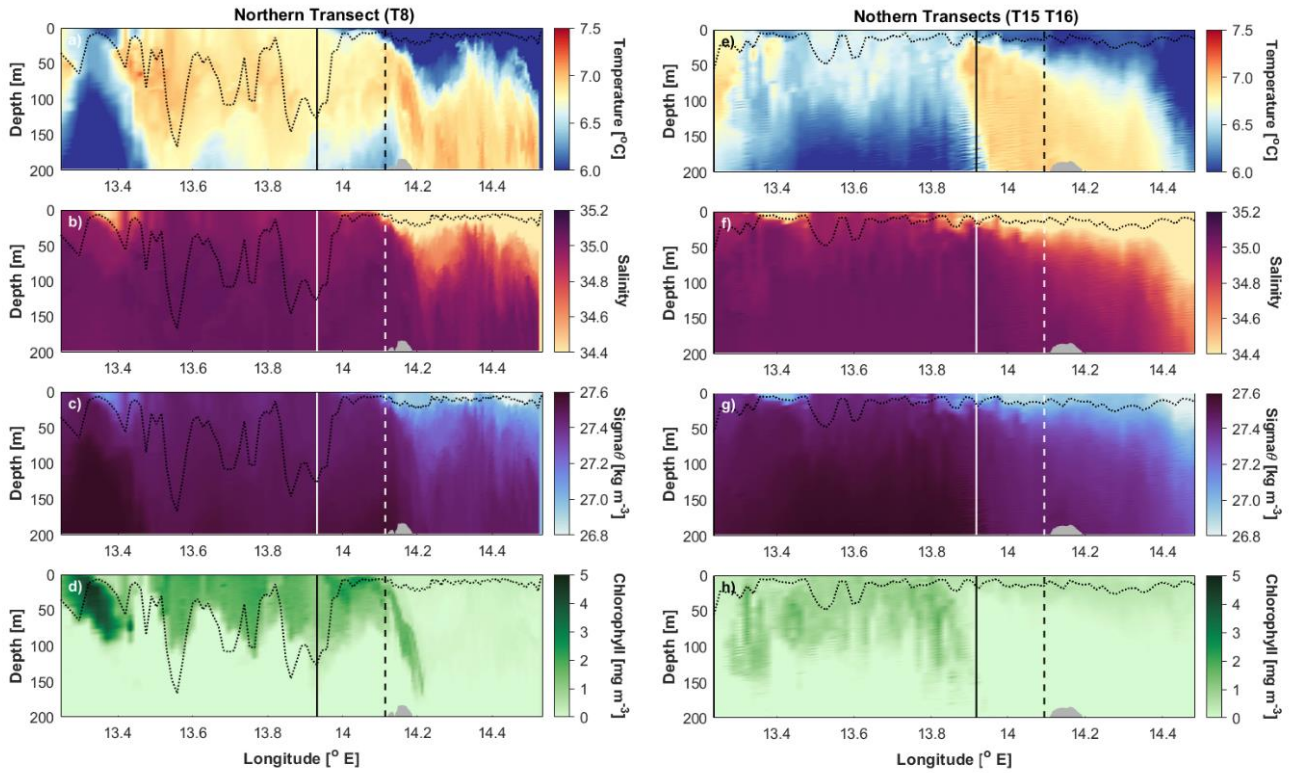
327 In the northern stations, mixed layer nitrate and silicic acid concentrations increased from the
328 shelf to deep waters. Mean mixed-layer nutrient concentrations in the southern shelf were lower
329 than at northern shelf stations, and both phosphate and silicic acid concentrations were
330 significantly lower than at the northern shelf stations as well ($p < 0.05$, Table 1, Table S2).

331 3.2 Phytoplankton distributions

332



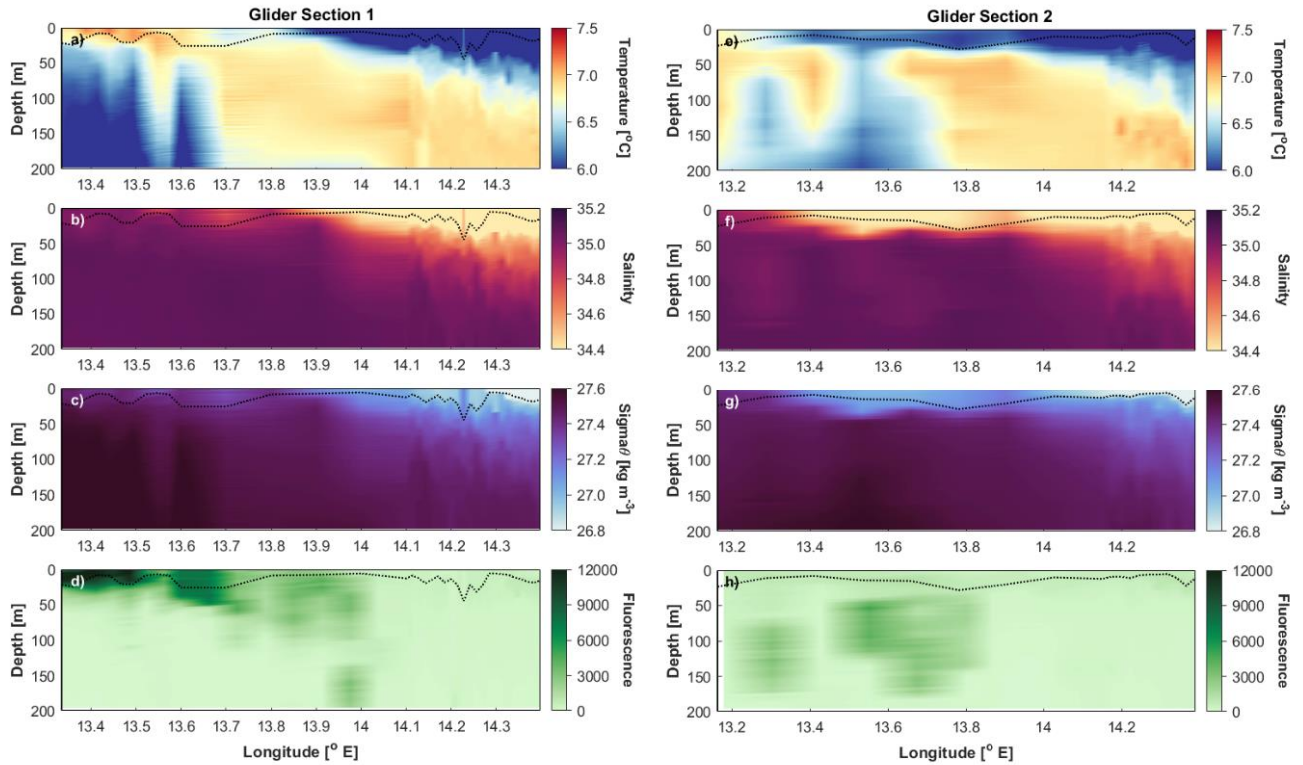
333
 334 **Figure 2.** Distribution of temperature, salinity, density (expressed as σ_θ) and chlorophyll in the
 335 upper 200 m within Transects 3-5 and Transect 2. Data from Transects 3-5 merged into a
 336 single mean distribution due to the closeness in time of sample collection. The dashed and solid
 337 lines represent the 200 and 1,000 m locations. The dotted line represents the depth of the mixed
 338 layer.
 339



341

342 **Figure 3.** Distribution of temperature, salinity, density (expressed as σ_θ) and chlorophyll in the
 343 upper 200 m within Transect 8 and Transect 15-16. Data from Transects 15 and 16 merged into
 344 a single mean distribution due to the closeness in time of sample collection. The dashed and solid
 345 lines represent the 200 and 1,000 m locations. The dotted line represents the depth of the mixed
 346 layer.

347



348

349 **Figure 4.** Distribution of temperature, salinity, density (expressed as σ_θ) and fluorescence in the
 350 upper 200 m within Glider Transects 1 and 2. Fluorescence expressed in arbitrary units. The
 351 dotted line represents the depth of the mixed layer.

352

353 The climatology derived from remotely-sensed chlorophyll *a* data showed that phytoplankton

354 blooms are usually initiated along the coast and move progressively offshore, and were separated

355 by less than a few weeks (Figure 5). Similarly, blooms also occurred earliest in the south and

356 spread northward, reaching a maximum in mid-April. Substantial spatial variability in the timing

357 of bloom appearance was noted, with a few locations offshore showing earlier growth and

358 accumulation than much of the rest of offshore waters. Only one clear-sky image was available

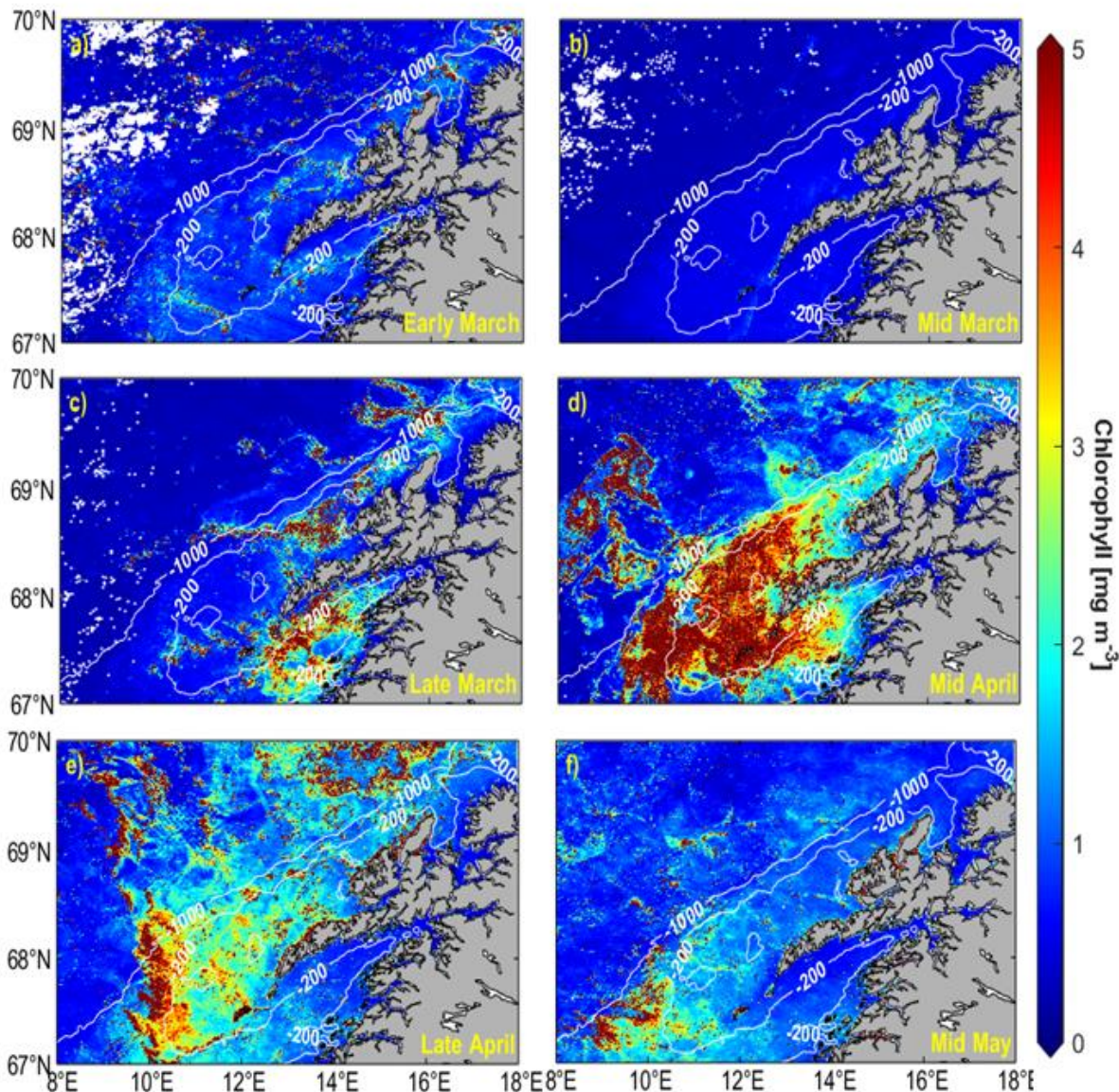
359 during the cruise (Figure. 6). It showed that waters on the continental shelf had lower chlorophyll

360 levels than those of offshore waters, which exhibited broadly distributed concentrations greater

361 **Table 1.** Mean mixed layer (Z_{mix}) concentrations of nitrate (NO_3^-), phosphate (PO_4^{3-}), silicic acid ($Si(OH)_4$), and euphotic zone average
362 concentrations of chlorophyll (chl a), particulate organic carbon (POC), particulate organic nitrogen (PON), and biogenic silica (BSi)
363 (and their standard deviations) off the northern Norwegian coast. Stations grouped by location and depth (shelf < 200 m; shelf break
364 200 - 400 m; slope 400 – 1,000 m; deep water > 1,000 m).

Location	Z_{mix} (m)	NO_3^- (μM)	PO_4^{3-} (μM)	$Si(OH)_4$ (μM)	Chl <i>a</i> ($mg\ m^{-3}$)	POC ($\mu mol\ L^{-1}$)	PON ($\mu mol\ L^{-1}$)	BSi ($\mu mol\ L^{-1}$)
Southern shelf (St. 7, 8)	13 ± 2.8	0.35 ± 0.05	0.09 ± 0.03	0.58 ± 0.01	$0.67 \pm 0.31^*$	1.84 ± 0.16	0.36 ± 0.09	3.55 ± 0.19
Northern shelf (St. 3, 4, 11, 14, 17-19, 23, 28)	22 ± 8.5	1.87 ± 1.11	0.24 ± 0.07	0.97 ± 0.23	$0.59 \pm 0.28^*$	1.29 ± 0.69	0.23 ± 0.14	3.89 ± 1.13
Northern shelf break (St. 9, 16)	13 ± 6.3	0.61 ± 0.56	0.51 ± 0.22	0.60 ± 0.14	0.45 ± 0.04	2.59 ± 2.03	0.49 ± 0.44	3.28 ± 0.18
Northern slope (St. 2, 6, 12, 15, 20, 22, 24, 27)	17 ± 4.2	1.68 ± 0.68	0.30 ± 0.23	1.35 ± 0.49	$1.62 \pm 1.57^*$	2.00 ± 1.49	0.31 ± 0.20	5.61 ± 3.95
Deep water (St. 1, 5, 10, 13, 21, 25, 26)	33 ± 16.0	3.04 ± 2.13	0.28 ± 0.10	1.54 ± 0.67	$2.19 \pm 1.35^*$	2.86 ± 2.01	0.58 ± 0.36	6.67 ± 3.53

365 *: some discrete samples lost; values estimated from CTD fluorescence data



366
 367 **Figure 5.** Seasonal chlorophyll climatologies generated from satellite imagery. A) early March
 368 (March 1-10), b) mid-March (March 11-20), c) late March (March 21 -31) , d) mid-April (April
 369 11 – 20), e) late April (April 21 – 30), and f) mid-May (May 11-20). Data were binned into 10-
 370 day intervals.
 371

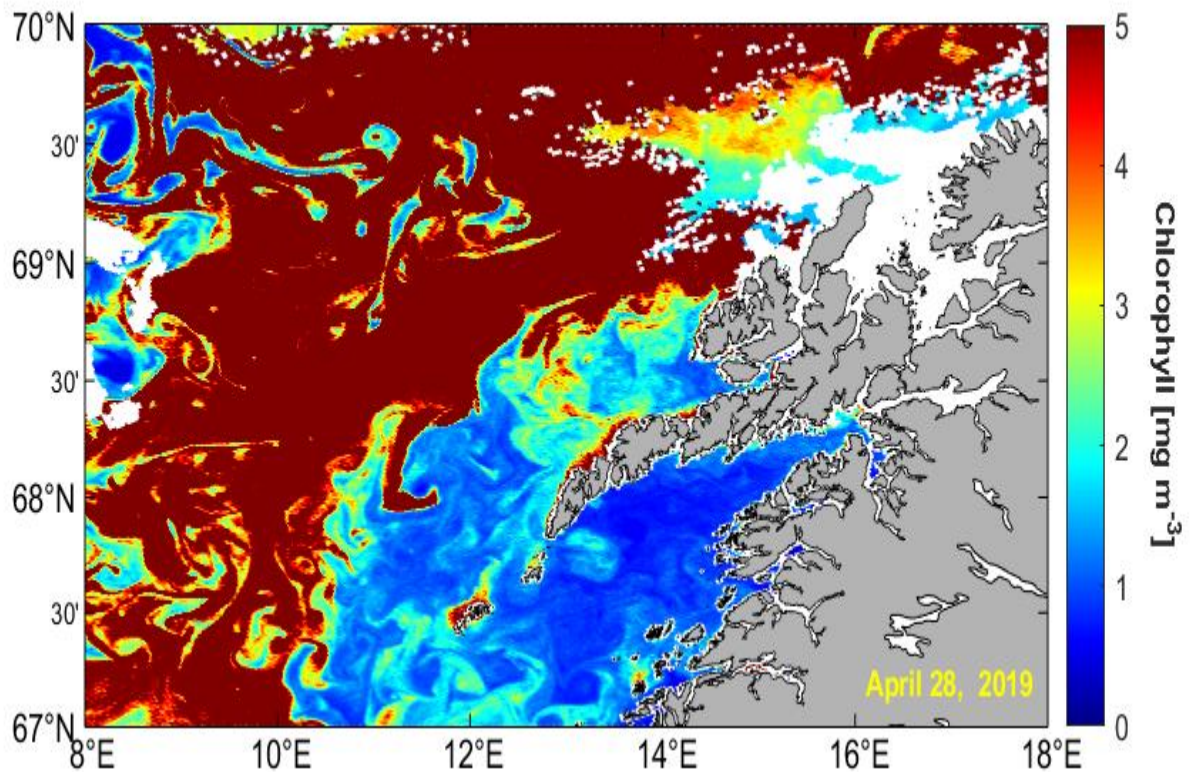


Figure 6. MODIS image of chlorophyll concentrations in the study area on April 28, 2019.

than 5 mg m^{-3} . Our maximum observed values (measured in offshore waters) were similar with those found in the climatology (ca. 5 mg m^{-3} ; Figures 2,3,4) and the April 26 image (Figure 6).

Euphotic zone depths ranged between 19 and 50 m (Table S2) and were shallower in deep-water stations ($27 \pm 6.4 \text{ m}$) relative to shelf-break and inshore stations (Table 2). Surface chl *a* concentrations ranged between $0.27\text{-}5.68 \text{ mg m}^{-3}$, and surface POC, PON and BSi ranged between $0.72 - 8.95$, $0.12 - 1.49$ and $2.15 - 22.5 \text{ mmol m}^{-3}$, respectively (Table S2). Average mixed layer chl *a*, POC, PON and BSi concentrations all tended to increase along an inshore-offshore gradient, and BSi concentrations suggested that phytoplankton were dominated by diatoms. Average mixed layer nitrate and silicic acid also showed a similar pattern. This suggests that the spring bloom, especially that on the continental shelf, had largely occurred prior to our observations and that

386 blooms developed in offshore waters during late April and early May, consistent with the satellite
387 climatology and the single image available (Figures 5, 6). BSi concentrations ranged between 1.34
388 and $22.5 \mu\text{mol L}^{-3}$; C/N molar ratios in the surface water ranged between 3.31 and 8.17, and
389 averaged 6.08 ± 1.54 for all euphotic zone samples. Surface POC/chl *a* ratios ranged between 10.9
390 and 77.5. Inshore waters had higher POC/chl *a* ratios than offshore waters (Table S2).

391 3.2.1 Temporal distributions

392 The highest chlorophyll concentrations were observed in offshore waters within transect T2
393 (April 25), and they tended to decrease through time, consistent with the climatology. Such
394 changes might be caused in part by the decrease in strength of the shelf break salinity front with
395 time, which likely resulted from the disruption of the transport barrier in late spring by eddy
396 activity (Dong et al., 2021). Surface chlorophyll concentrations also decreased through time and
397 became concentrated at depth (usually at the base of the mixed layer). The depth of maximum chl
398 *a* concentrations also deepened through time (Figure 2). Integrated euphotic zone chlorophyll
399 concentrations generally decreased with time as well, although the trend was most obvious at deep-
400 water stations (Table S2). Glider fluorescence doubled offshore in the transect sampled starting on
401 April 28 (Figure 4), and shelf fluorescence was low within both occupations.

402 3.2.2 Spatial distributions

403 Surface and integrated euphotic zone chlorophyll *a* concentrations ranged between 0.27 and
404 5.68 mg m^{-3} and 7.65 and 104 mg m^{-2} , respectively; stations located in the northern NAW showed
405 significantly greater concentrations (both at the surface and in integrated values) than the NCW
406 stations ($p < 0.001$, Table S2). Chlorophyll *a* concentrations observed by the MVP were higher in
407 offshore waters than inshore on all transects regardless of the date of sampling (Figures 2, 3).
408 Fluorescence observed by the glider also showed the same trend (Figure 4). Maximum Chl *a*

409 concentrations occurred within mixed layer in offshore waters, but below the mixed layer in the
 410 inshore waters on transects T2, T3, T4, T5 and T8 (Figures 2, 3). Compared with transect T8, both
 411 mixed layer depth and chl *a* concentrations decreased within transects T15 and T16 (sampled six
 412 days later; Figure 4).

413 3.3 Primary productivity

414 Primary productivity was lowest on the continental shelf and increased in deeper waters,
 415 regardless of the method of estimation (Table 2). In general productivity estimated by the vertically
 416 resolved model was less than that determined from surface properties (Table 2). The two estimates
 417 were significantly correlated ($R^2=0.90$, $p<0.001$), with the surface estimates being 29% higher on
 418 average than the vertically resolved model. Surface primary productivity ranged between 9 - 284

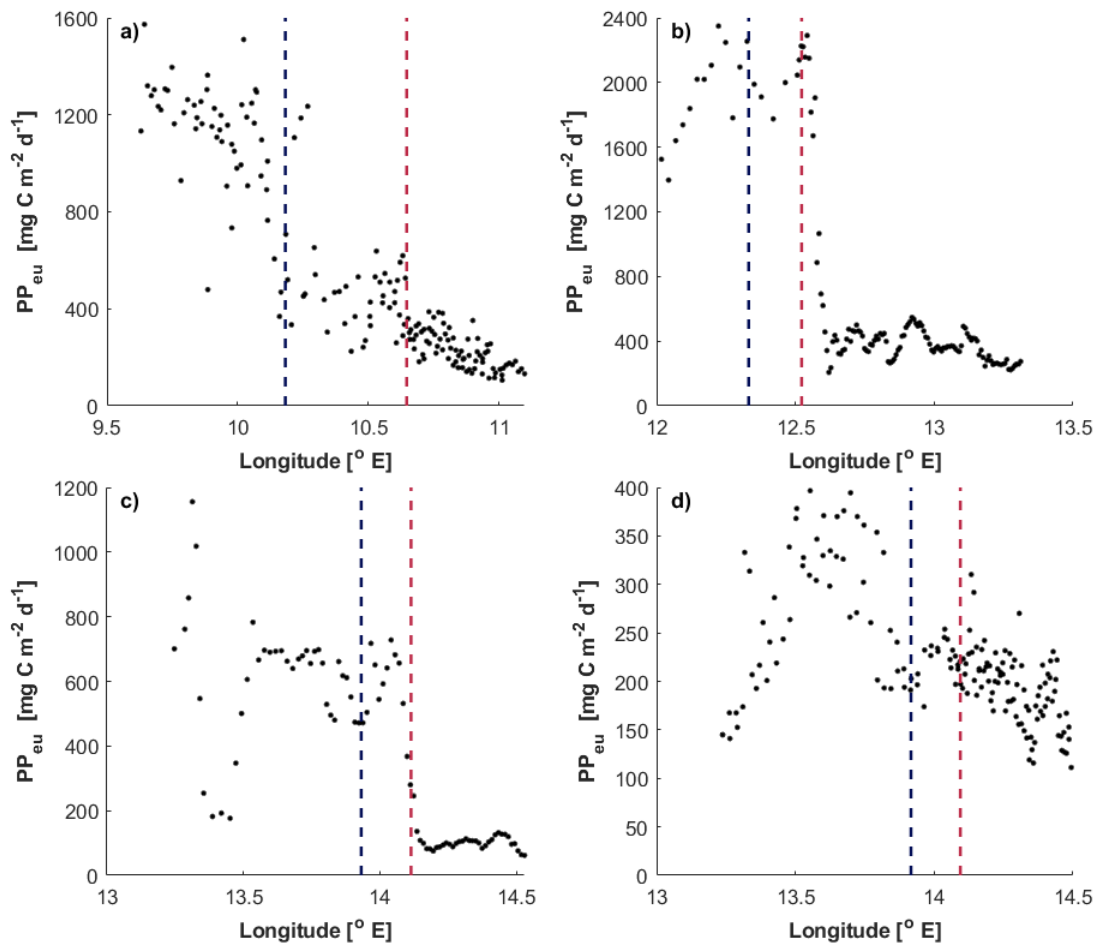
419 **Table 2.** Mean euphotic zone depths (Z_{eu} , 1% isolume) and modeled primary productivity (and
 420 standard deviations) off the Norwegian coast. Stations grouped by location (south and north) and
 421 depth (shelf < 200 m; shelf break 200 – 400 m; slope 400 – 1,000 m; deep water > 1,000 m). PP1
 422 is the euphotic zone integrated primary productivity based on the vertically resolved model (Eq.
 423 1 and 2); PP2 is based on Eq. 3.

Location	Z_{eu} (m)	PP1 (mg C m ⁻² d ⁻¹)	PP2 (mg C m ⁻² d ⁻¹)
Southern shelf (St. 7, 8)	33 ± 2.8	217 ± 30	458 ± 18
Northern shelf (St. 3, 4, 11, 14, 17-19, 23, 28)	34 ± 9.0	216 ± 87	460 ± 167
Northern shelf break (St. 9, 16)	43 ± 7.8	196 ± 24	472 ± 73
Northern slope (St. 2, 6, 12, 15, 20, 22, 24, 27)	32 ± 7.3	513 ± 558	937 ± 778
Deep water (St. 1, 5, 10, 13, 21, 25, 26)	27 ± 6.4	660 ± 327	1,357 ± 739

424 **Table 3.** Means and standard deviations of net seasonal drawdown of nitrate and silicic acid and
 425 the derived net community production (NCP) derived from nitrate and silicic acid removal (ΔNO_3
 426 and $\Delta Si(OH)_4$) off the Norwegian coast as determined from seasonal nitrate and silicic acid
 427 deficits of the upper 50 m of the water column (Eq. 4). NCP_{Si}/NCP_N is the percentage of NCP
 428 attributable to diatoms. Stations grouped by location (south and north) and depth (shelf < 200 m;
 429 shelf break 200 – 400 m; slope 400 – 1,000 m; deep water > 1,000 m).

Location	ΔNO_3 (μM)	$\Delta Si(OH)_4$ (μM)	NCP_N ($mg\ C\ m^{-2}\ d^{-1}$)	NCP_{Si} ($mg\ C\ m^{-2}\ d^{-1}$)	NCP_{Si}/NCP_N (%)
Southern shelf (St. 7, 8)	304 ± 80.9	157 ± 15.7	34.4 ± 7.91	20.5 ± 2.04	63
Northern shelf (St. 3, 4, 11, 14, 17-19, 23, 28)	212 ± 78.4	127 ± 21.8	21.7 ± 9.35	12.9 ± 3.07	60
Northern shelf break (St. 9, 16)	313 ± 32.3	153 ± 19.6	32.1 ± 4.69	15.6 ± 2.68	49
Northern slope (St. 2, 6, 12, 15, 20, 22, 24, 27)	167 ± 70.7	94.7 ± 31.5	21.7 ± 9.35	12.9 ± 3.07	57
Deep water (St. 1, 5, 10, 13, 21, 25, 26)	327 ± 73.2	133 ± 26.1	33.4 ± 8.98	13.6 ± 3.16	41

430
 431 $mg\ C\ m^{-3}\ d^{-1}$ (Table S2) and was significantly greater in the stations located in NAW ($p < 0.001$,
 432 Table S2). Primary productivity also was estimated along the MVP transects and ranged from 62
 433 - 2,350 $mg\ C\ m^{-2}\ d^{-1}$ (Figure 7). Productivity was greatest in deep water and was reduced on the
 434 shelf in all 7 transects. Seasonal production estimated from nutrient deficits was much less than
 435 that estimated from the bio-optical models (Table 3). It was broadly similar throughout the
 436 region, but slightly less on the northern shelf, where nutrients were remaining in the surface layer



437

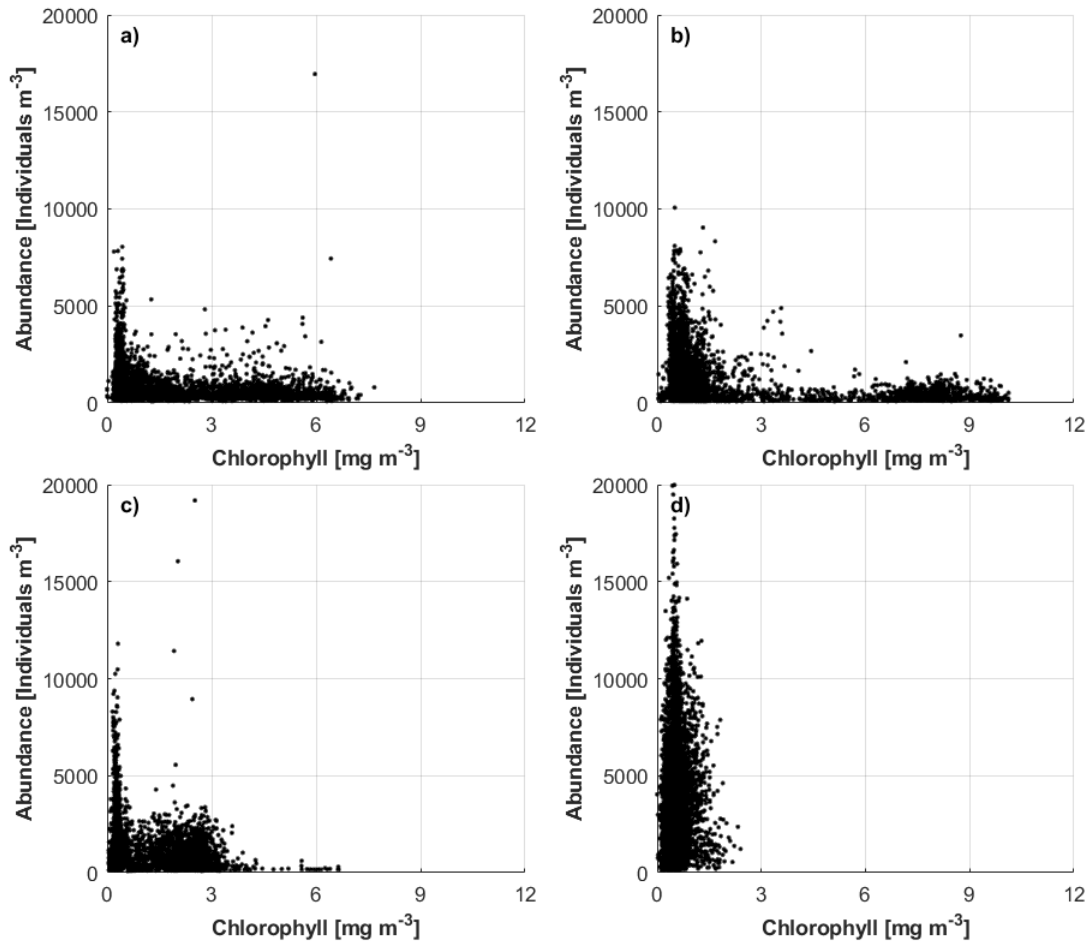
438 **Figure 7.** Integrated primary productivity estimated from the moving vessel profiler from the
 439 vertically resolved model. a) transects T3, T4 and T5; b) transect T2; c) transect T8; d) transects
 440 T15 and T16. Red and blue dashed lines represent 200 and 1000 m.

441

442 and fueling active growth. Estimates of diatomaceous production were from 41 – 63% of total net
 443 community production, confirming the important role of diatoms in the spring bloom.

444 3.4 Relationship between zooplankton and phytoplankton distribution

445 The highest *C. finmarchicus* abundance within the 1.0-2.0 mm ESD size fraction was ca.
 446 20,000 individuals m^{-3} and was found in the northern transects 15 and 16 (Figure 8d). *C.*
 447 *finmarchicus* abundance in the earlier transects was about a half that found in T15 and T16, with



448

449 **Figure 8.** Relationship between copepod abundance as estimated from particle abundance
 450 between 1 and 2 mm ESD in the upper 30 m and chlorophyll in a) transects T3, T4 and T5; b)
 451 transect T2; c) transect T8; d) transects T15 and T16.

452

453 maxima reaching ca. 10,000 individuals m^{-3} (Figure 8a,b,c). *C. finmarchicus* abundance maxima

454 were associated with low chlorophyll concentrations in all transects.

455

456 4 Discussion

457 4.1. Spatial and Temporal Variability of Norwegian Coastal Waters

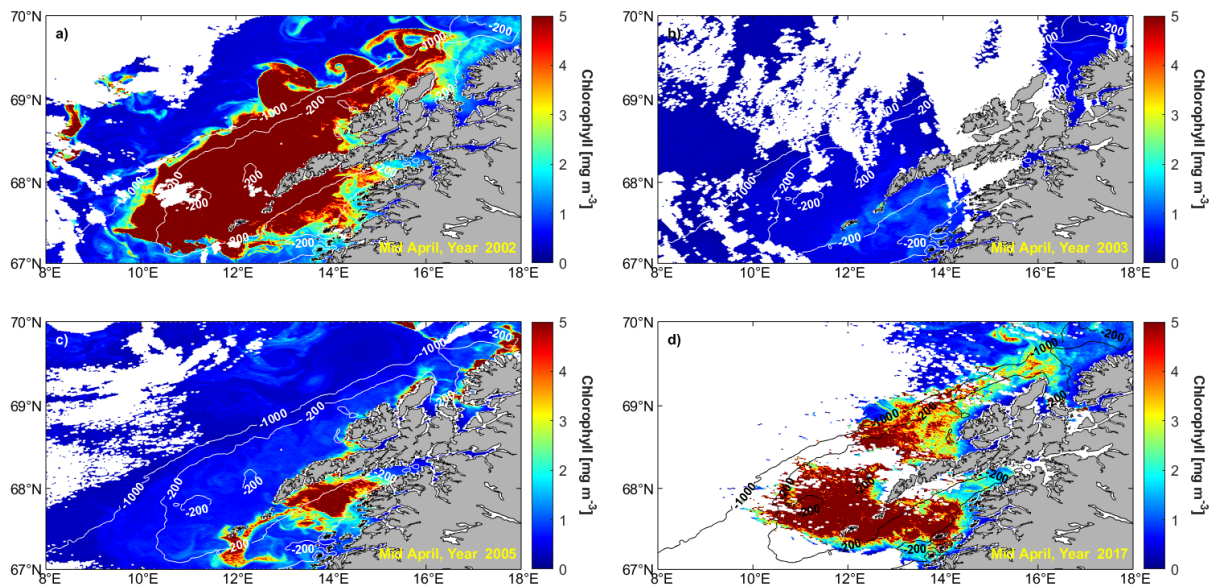
458 Phytoplankton off the northern Norwegian coast exhibited substantial spatial variability that
459 reflected the rapid growth and accumulation within the sub-polar spring bloom. Despite the
460 relatively short sampling period, the use of multiple sampling modes allowed us to characterize
461 the state of the bloom over broad areas. The satellite climatology clearly showed the temporal and
462 spatial scales of variability (Figure 5). Satellite-derived chlorophyll concentrations were low
463 through March, but increased substantially by mid-April to concentrations greater than 5 mg m^{-3} .
464 These increases were largely confined to the continental shelf in waters that likely had increased
465 stratification resulting from land-based inputs of fresher water. The high chlorophyll
466 concentrations on the shelf were reduced rapidly (over ca. two weeks) but remained $> 2 \text{ mg m}^{-3}$
467 over broad areas of the shelf. Some areas in deep water also exhibited high chlorophyll
468 concentrations in mid-April, and these may have resulted from the advective transport of
469 phytoplankton when the density barrier at the shelf break was disrupted due to increased eddy
470 activity during this period (Dong et al., 2021).

471 Waters on the continental slope and deeper areas supported the growth and accumulation of
472 phytoplankton later than those on the shelf. This is clearly shown by the climatology, the single
473 image obtained during our field observations, and the field measurements themselves.
474 Concentrations of chlorophyll to the west of the shelf break were substantial ($> 5 \text{ mg m}^{-3}$) and
475 equal to those that occurred earlier on the continental shelf. Thus, any transfer of primary
476 production through the food web would be similar in both regions and not simply confined to
477 shallow waters, despite the differing phenology of the two areas.

478 The climatology does not address aspects of interannual variability, which is also substantial
479 (Figure 9). Such variability potentially can influence the coupling between phyto- and zooplankton
480 and could have broad food-web implications. That is, some years the physical-biological coupling

481 could be strong and facilitate an efficient transfer of organic matter to higher trophic levels, but in
 482 other years the reduced coupling could weaken such transfers. Understanding the magnitude of
 483 such variability and the strength of the biophysical coupling can contribute to the effective
 484 management of Norwegian fisheries.

485 Primary productivity in the region is substantial, but also shows the same variability as shown
 486 by chlorophyll distributions. This is not surprising, as the estimates derived from the bio-optical
 487 model are dependent on chlorophyll concentrations. Very few direct productivity measurements
 488 have been reported from this area, which is surprising given the importance of quantifying the
 489 input of organic matter into *Calanus*-based food webs. The vertically resolved model provided
 490



491 **Figure 9.** Examples of interannual variability in chlorophyll concentrations off the Lofoton
 492 coast. All images are from approximately the same date in mid-April. a) 2002, b) 2003, c) 2005,
 493 and d) 2017.
 494
 495

496 estimates that were ca. 70% of those derived from the surface chlorophyll-derived method.
 497 Maximum productivity was greater than $2 \text{ g C m}^{-2} \text{ d}^{-1}$, consistent with the few direct estimates of
 498 productivity in the region (Wassmann & Aadnesen, 1984; Paashe, 1986) and of other sub-polar

499 systems (Harrison et al., 2013; Richardson & Bendtsen, 2021). We believe the estimates derived
500 from the vertically resolved model (PP1; Table 2) are more likely closer to the realized productivity
501 due to the inclusion of the photoinhibition term, which is not included in surface chlorophyll-
502 derived estimates (PP2; Table 2). The strength of the density front impacted the magnitude of
503 changes from shelf water to deep water, as productivity was much greater offshore during periods
504 when a steep physical front was present (Figure 7b,c), whereas it increased gradually in transects
505 with a reduced physical front (Figures 6a,d). Overall, these rates demonstrate the productive nature
506 of the Norwegian shelf-slope region during spring.

507 4.2 Relationship between Chlorophyll Concentrations and Zooplankton

508 The spatial and temporal variability of the region was also expressed in the relationship
509 between chlorophyll concentrations and *Calanus finmarchicus* abundance. Within a spring bloom,
510 zooplankton biomass lags behind phytoplankton growth and accumulation due to the effects of
511 temperature on zooplankton development (Cushing, 1995; Søreide et al., 2010; Daase et al., 2013).
512 Hence, at any time phytoplankton and zooplankton can be negatively (phytoplankton increasing
513 when zooplankton biomass is low, or when zooplankton are high and phytoplankton levels have
514 been reduced) or positively (when both are increasing) correlated. This relationship appears to be
515 expressed in our data (Figure 8, Table S2). In the earliest occupation (Transect 2, April 29),
516 chlorophyll on the shelf was relatively low, and zooplankton abundance was relatively uniform
517 over the entire transect, although zooplankton maxima occurred in low chlorophyll waters (Figure
518 8a). This may represent a period when phytoplankton biomass in the upper 30 m had been reduced
519 either by grazing or sinking to depth. Chlorophyll maxima were located below 30 m, suggesting
520 that passive sinking may have been the dominant mechanism in removing phytoplankton from the
521 surface layer. The next day (April 30, Transects 3-5), there were a number of depths where the low

522 chlorophyll-elevated zooplankton abundance relationship was observed, suggesting a period
523 where zooplankton biomass had increased and phytoplankton chlorophyll had decreased (Figure
524 8b). Chlorophyll maxima were again located below the mixed layer, suggesting the bloom was in
525 the process of passively sinking to depth, and that the inverse relationship was not a direct result
526 of grazing. Six days later (Transect 8, May 5; Figure 8c), the pattern was similar to that found on
527 April 30 – relatively enhanced zooplankton abundance associated with lower fluorescence,
528 although there was a broader distribution of higher chlorophyll than in the south. Within
529 Transects 15-16 (May 10-11), the relationship was notably different, in that there were no
530 chlorophyll concentrations $> 2.4 \text{ mg m}^{-3}$ and zooplankton biomass was elevated over much of the
531 transect (Figure 8d). We suggest that growth of both zooplankton and phytoplankton were more
532 tightly coupled at this time and location. Given the spatio-temporal variability that occurs
533 throughout the region, understanding the coupling between phytoplankton and zooplankton is
534 challenging.

535 Given that *Calanus finmarchicus* reaches such massive accumulations to allow it to be
536 observed by satellites (Basedow et al., 2019; Dong et al., 2021), we hypothesized that the copepod
537 populations could exert a substantial influence on phytoplankton biomass. Irigoien et al. (1998)
538 sampled from March – June in the deep waters off Norway and estimated that *C. finmarchicus*
539 used ca. 15% of the chlorophyll per day during the bloom period (chlorophyll concentrations up
540 to 3 mg Chl m^{-3}) and 5% per day post-bloom. Using the average ingestion rate they determined
541 ($7.59 \text{ ng C individual}^{-1} \text{ d}^{-1}$) and their mean C/chl ratio of 62 (Irigoien et al., 1998) together with the
542 mean abundances of *C. finmarchicus* we found in the upper 30 m along all MVP transects, we
543 estimate that *Calanus* grazing could remove from 0.06 to $14.8 \text{ mg chl m}^{-3} \text{ d}^{-1}$ (Table 4). Converting
544 our production rates into chlorophyll units, we further estimate that the average percentage of

545 **Table 4.** Estimates of potential chlorophyll removal (Chl_{rem}) by *Calanus finmarchicus* grazing
 546 on each MVP transect. Ingestion rate used was $7.59 \text{ ng C ind}^{-1} \text{ d}^{-1}$ (Irigoien et al., 1998) and were
 547 converted into chlorophyll units using their C/chl ratio of 62. Chlorophyll concentrations (Chl)
 548 and *C. finmarchicus* abundances are the means in the upper 30 m determined from fluorescence
 549 and the LOPC. Chlorophyll production (Chl_{prod}) rates were calculated from the productivity of
 550 each descent of the MVP estimated from the vertically resolved model and converted into
 551 chlorophyll units using a C/chl ratio of 40. Daily removal is the percentage of the chlorophyll
 552 removed relative to the total chlorophyll pool (initial plus production). Production/Removal is
 553 the ratio of Chl_{prod} and Chl_{rem} ; values > 1 indicate that chlorophyll concentrations were
 554 increasing.

Transect	Chl (mg m^{-3})	<i>Calanus</i> Abundance (ind m^{-3})	Chl_{prod} (mg chl m^{-2} d^{-1})	Chl_{rem} (mg chl m^{-2} d^{-1})	Daily Removal (%)	Production/ Removal
3	1.89	678	5.81	2.49	7.84	5.55
4	1.89	380	31.8	0.06	0.08	1252
2	2.12	1017	8.49	3.73	12.1	6.22
8	1.13	1038	14.5	3.81	18.3	9.16
15	0.58	4036	4,21	14.8	72.9	0.42
16	0.53	2811	5.13	10.3	51.3	1.03

556
 557 removal in Transects 2 – 8 (all completed before May 5) was less than 10%, while in the two
 558 northern transects (15 and 16, sampled on May 10-11) daily removal averaged 62%. Removal
 559 largely varies with *Calanus* abundance, which was higher in the north. These estimates have
 560 substantial uncertainty, given the variability in productivity and carbon/chlorophyll ratios within
 561 each transect, and their potential changes in time. As a result, caution needs to be used in
 562 extrapolating them to broader regions. To better understand the impact of *Calanus* grazing under
 563 conditions of extreme biomass accumulations, estimates of ingestion rates, phytoplankton growth
 564 and biomass, and copepod abundance need to be completed at the same time and location.

565 The variability of estimated *Calanus* removal of chlorophyll within a single transect was also
566 substantial. For example, within Transect 8 the daily removal range from 0.08 to 196%, with
567 similar ranges at other transects (data not shown). As removal is largely controlled by *Calanus*
568 abundance, this suggests that other factors are influencing the sub-mesoscale distributions of the
569 copepod, such as vertical migration, movement in response to predation, and responses to other
570 environmental parameters. The sub-mesoscale distributions of copepods may have a strong
571 influence on the trophic dynamics of the Norwegian shelf-slope region and deserves greater
572 attention using modern assessments of biomass.

573 Another estimate of the impact of zooplankton on phytoplankton distributions can be obtained
574 by combining the productivity rates and the particulate matter distributions to calculate the daily
575 increase in POC (and chlorophyll), and comparing those estimates with the chlorophyll loss rates
576 estimated by Irigoien et al. (1998). By estimating phytoplankton growth rates from the ratio of
577 productivity and POC concentrations, and assuming exponential growth over one day, the increase
578 in POC can be approximated (Table S4). The mean daily per cent increase in POC is more than
579 86%, almost equal to a doubling per day [consistent with the high primary productivity rates]. If a
580 similar calculation is made using chlorophyll data (by converting the carbon production rates to
581 chlorophyll production rates using a C:chl ratio of 40; Rieman et al., 1989), the mean percentage
582 increase is about 34%, less than that derived using carbon values (Table S4), due to the low C:chl
583 ratios we occasionally observed. Regardless, Irigoien et al. (1998) estimated daily chlorophyll loss
584 rates of 15% at stations with chlorophyll concentrations greater than 3 mg m^{-3} , and 5% at stations
585 with chlorophyll concentrations less than 3 mg m^{-3} . Our results strongly suggest that changes in
586 chlorophyll and particulate organic carbon concentrations are not being regulated by the grazing
587 activities of copepods, despite the substantial abundances of *C. finmarchicus*.

4.3. Controls on the vertical distribution of chlorophyll

Vertical chlorophyll maxima were consistently found associated with density discontinuities. Such maxima can have multiple mechanisms of formation (Cullen, 2015), but given the time scales of our sampling, we suggest that acclimation to low irradiance levels in the deep chlorophyll maximum is less likely than physical accumulation via passive sinking of cells, whose sinking rates may have been enhanced by nutrient limitation. The stations in the southern shelf (Transect T2; Figure 2) likely had elevated concentrations prior (ca. 2 weeks) to our arrival, and the chlorophyll maxima we observed were located below the mixed layer. Within Transects 3-5 chlorophyll on the shelf was largely associated with the base of the mixed layer (Figure 2); during Transect 8 and Transects 15-16 the shelf chlorophyll did not show substantial vertical maxima, but the deep water stations within Transect 8 had high chlorophyll concentrations within the mixed layer, whereas within Transects 15-16 the chlorophyll was distributed below the mixed layer over a broad depth range (from 50-150 m; Figure 3), similar to Transect T2. The strong flux of chlorophyll to depth in Transects 2 and 8 at depths < 200 m were likely driven by mesoscale motions (Zhong et al., unpublished). These patterns suggest that vertical phytoplankton distributions are largely controlled by passive sinking rather than the effects of grazing. Further observations and direct measurements of sinking and grazing are required to determine the relative magnitude of chlorophyll removal by micro- and mesozooplankton and physical processes in northern Norwegian waters fully understand the role of grazing on phytoplankton distributions.

6 Conclusions

We characterized the northern Norwegian continental shelf/coast region with regard to phytoplankton distributions and its relationship to the dominant grazer, *Calanus finmarchicus*.

611 The region is characterized by a spring bloom that first occurs on the shallow waters of the
612 continental shelf, likely due to increased stratification by fresh-water inputs from land, and
613 proceeds northward and offshore over times scales of a few weeks. Substantial spatial and temporal
614 variability occurs on all scales, which can potentially have important impacts on regional food
615 webs. The coupling of phytoplankton and zooplankton also varies spatially. Primary productivity
616 is substantial and follows patterns similar to those of chlorophyll, and diatoms contributed a
617 majority of the net community production. *Calanus finmarchicus*, the dominant grazer in the
618 system, potentially removes from <1 to 78% of the chlorophyll per day. However, chlorophyll
619 appears to sink from the euphotic zone and is redistributed below the mixed layer, suggesting that
620 chlorophyll losses from copepod grazing influence phytoplankton vertical distributions less than
621 passive sinking during this period.

622

623 **Acknowledgments, Samples, and Data**

624 This research was supported by grants from the National Science Foundation of China (Grant
625 41861134040) and the Norwegian Research Council (Grant 287043). The authors have no
626 conflicts of interest with these data. Ms. Yiwu Zhu assisted with the analysis of the optical plankton
627 counter data. We thank the officers and crew of the *R.V. Helmar Hanson* for their assistance, and
628 our Stressor colleagues for their help at sea. Nutrient and particulate matter concentration data
629 can be publicly accessed at <https://doi.org/doi:10.18710/KVPUTW>; moving vessel data (including
630 the LOPC data) can be accessed at <https://doi.org/doi:10.18710/DXA0F3>. A full cruise report is
631 available at <https://doi.org/doi:10.18710/KVPUTW>. The ocean color data, including VIIRS and
632 MODIS, were provided by the Ocean Biology Processing Group
633 (<https://oceancolor.gsfc.nasa.gov>).

634 **References**

- 635 Bagøien, E., Melle, W., & Kaartvedt, S. (2012). Seasonal development of mixed layer depths,
636 nutrients, chlorophyll and *Calanus finmarchicus* in the Norwegian Sea – A basin-scale habitat
637 comparison. *Progress in Oceanography*, *103*, 58-79.
638 <https://dx.doi.org/10.1016/j.pocean.2012.04.014>
- 639 Basedow, S.L., Edvardsen, A., & Tande, K.S. (2008). Vertical segregation of *Calanus*
640 *finmarchicus* copepodites during the spring bloom. *Journal of Marine Systems*, *70*, 21-32.
641 <https://doi.org/10.1016/j.jmarsys.2007.02.023>
- 642 Basedow, S. L., Tande, K. S., Norrbin, M. F., & Kristiansen, S. A. (2013). Capturing quantitative
643 zooplankton information in the sea: Performance test of laser optical plankton counter and
644 video plankton recorder in a *Calanus finmarchicus* dominated summer situation. *Progress in*
645 *Oceanography*, *108*, 72-80. <https://doi.org/https://doi.org/10.1016/j.pocean.2012.10.005>
- 646 Bates, N.R., Hansell, D.S., Carlson, C.A., & Gordon, L.I. (1998). Distribution of CO₂ species,
647 estimates of net community production and air–sea CO₂ exchanges in the Ross Sea polynya.
648 *Journal of Geophysical Research*, *103*, 2883–2896.
- 649 Behrenfeld, M.J. & Falkowski, P.G. (1997a). Photosynthetic rates derived from satellite-based
650 chlorophyll concentration. *Limnology and Oceanography*, *42*, 1–20.
- 651 Behrenfeld, M.J. & Falkowski, P.G. (1997b). A consumer’s guide to phytoplankton primary
652 productivity models. *Limnology and Oceanography*, *42*, 1479–1491.
- 653 Bouman, H.A., Platt, T., Doblin, M., Figueriras, F.G., Gudmundsson, K., Gudfinnsoson, H.G., et
654 al. (2018). Photosynthesis-irradiance parameters of marine phytoplankton: synthesis of a
655 global data set. *Earth Systems Science Data*, *10*, 251–266. [https://doi.org/10.5194/essd-10-](https://doi.org/10.5194/essd-10-251-2018)
656 [251-2018](https://doi.org/10.5194/essd-10-251-2018)

- 657 Brzezinski, M.A. (1985). The Si:C:N ratio of marine diatoms: interspecific variability and the
658 effect of some environmental variables. *Journal of Phycology*, 21, 347-357.
- 659 Brzezinski, M.A., & Nelson, D.M. (1989). Seasonal changes in the silicon cycle within a Gulf
660 Stream warm-core ring. *Deep-Sea Research*, 36, 1009–1030.
- 661 Cushing, D. (1995). *Population production and regulation in the sea: a fisheries perspective*,
662 Cambridge, UK: Cambridge Univ. Press.
- 663 Daase, M., Falk-Petersen, S., Varpe, Ø., Darnis, G., Søreide, J.E., et al. (2013). Timing of
664 reproductive events in the marine copepod *Calanus glacialis*: a pan-Arctic perspective.
665 *Canadian Journal of Fisheries and Aquatic Sciences*, 70, 871- 884.
- 666 Dong, H., Zhou, M., Hu, Z., Zhang, Zhong, Y., Basedow, S.L., & Smith, W.O., Jr. (2021).
667 Transport barriers and the retention of *Calanus finmarchicus* on the Lofoten shelf in early
668 spring. *Journal of Geophysical Research*, 126, e2021JC017408.
669 <https://doi.org/10.1029/2021JC017408>
- 670 Friedrichs, M.A.M., Carr, M.-E., Barber, R.T., Scardi, M., Antoine, D., Armstrong, R.A., et al.
671 (2009). Assessing the uncertainties of model estimates of primary productivity in the tropic
672 Pacific Ocean. *Journal of Marine Systems*, 76, 113-133.
- 673 Gaardsted, F., Tande, K.S., & Basedow, S. L. (2010). Measuring copepod abundance in deep-
674 water winter habitats in the NE Norwegian Sea: intercomparison of results from laser optical
675 plankton counter and multinet. *Fisheries Oceanography*, 19, 480-492.
676 <https://doi.org/10.1111/j.1365-2419.2010.00558.x>
- 677 Gardner, W.D., Richardson, M.J. & Smith, W.O., Jr. (2000). Seasonal patterns of water column
678 particulate organic carbon and fluxes in the Ross Sea, Antarctica. *Deep-Sea Research II*, 47,
679 3423–3449.

- 680 Herman, A., Beanlands, B., & Phillips, E. (2004). The next generation of optical plankton counter:
681 the laser-OPC. *Journal of Plankton Research*, 26, 1135-1145.
- 682 Irigoien, X., Head, R., Klenke, U., Meyer-Harms, B., Harbour, D., Niehoff, B., ... & Harris, R.
683 (1998). A high frequency time series at weathership M, Norwegian Sea, during the 1997
684 spring bloom: feeding of adult female *Calanus finmarchicus*. *Marine Ecology Progress Series*,
685 172, 127-137.
- 686 Kaufman, D.E., Friedrichs, M.A.M., Smith, W.O., Jr., Queste, B.Y., & Heywood, K.J. (2014).
687 Biogeochemical variability in the southern Ross Sea as observed by a glider deployment.
688 *Deep-Sea Research I*, 92, 93-106.
- 689 Lee, Z., Marra, J., Perry, M.J., & Kahru, M. (2015). Estimating oceanic primary productivity for
690 ocean color remote sensing: a stragic assessment. *Journal of Marine Systems*, 149, 50-59.
- 691 Ma, J., & Smith, W.O., Jr. (2022). Primary productivity in the Mid-Atlantic Bight: Is the shelf
692 break a location of enhanced productivity? *Frontiers in Marine Science*, 9, 824303.
693 <https://doi:10.3389/fmars.2022.824303>
- 694 Mahadevan, A., D'Asaro, E., Lee, C., Perry, M.J. (2012). Eddy-driven stratification initiates North
695 Atlantic spring phytoplankton blooms. *Science*, 337, 54-58.
- 696 Marra, J. (2009). Net and gross productivity: weighing in with ¹⁴C. *Aquatic Microbial Ecology*,
697 56, 123–131.
- 698 Marra, J. F., Barber, R.T., Barber, E., Bidigare, R.R., Chamberlin, W.S., Goericke, R., et al. (2021).
699 A database of ocean primary productivity from the ¹⁴C method. *Limnology and Oceanography*
700 *Letters*, 6, 107-111. <https://doi.org/10.1002/lol2.10175>

- 701 Morel, A. (1974). Optical properties of pure water and pure seawater. In N.G. Jerlov, E.
702 Steemann Nielsen (Eds.), *Optical Aspects of Oceanography* (pp. 1-24). San Diego, CA:
703 Academic.
- 704 Morel, A. (1998). Optical modeling of the upper ocean in relation to its biogenous matter content
705 (Case I Waters). *Journal of Geophysical Research*, *93*, 10,749-10,768.
- 706 Mork, M., Swallow, J.C., Currie, R.I., Gill, A E., & Simpson, J.H. (1981). Circulation phenomena
707 and frontal dynamics of the Norwegian coastal current. *Philosophical Transactions of the*
708 *Royal Society of London. Series A*, *302*, 635-647. <https://doi.org/10.1098/rsta.1981.0188>
- 709 Oliver, H., Zhang, W.G., Smith Jr., W.O., Alatalo, P., Chappell, P.D., Hirzel, A.J., et al. (2021).
710 Diatom hotspots driven by western boundary current instability. *Geophysical Research*
711 *Letters*, *48*, e2020GL091943, <https://doi.org/10.1029/2020GL091943>
- 712 Paasche, E. (1986). Pelagic primary production in near shore waters. In T.H. Blackburn, J.
713 Sørensen (Eds.), *Nitrogen Cycling in Coastal, Marine Environments* (pp. 33-57). New York:
714 John Wiley.
- 715 Platt, T. & Jassby, A.D. (1976). The relationship between photosynthesis and light for natural
716 assemblages of coastal marine phytoplankton. *Journal of Phycology*, *12*, 421–430.
- 717 Pedersen, O., Zhou, M., Tande, K., & Edvardsen, A. (2005). Eddy formation on the coast of North
718 Norway—evidenced by synoptic sampling. *ICES Journal of Marine Science*, *62*, 615-628.
- 719 Richardson, K., & Bendtsen, J. (2021). Distinct seasonal primary production patterns in the sub-
720 polar gyre and surrounding seas. *Frontiers of Marine Science*, *8*, 785685.
721 <https://doi:10.3389/fmars.2021.785685>

- 722 Riemann, B., Simonsen, P., & Stensgaard, L. (1989). The carbon and chlorophyll content of
723 phytoplankton from various nutrient regimes. *Journal of Plankton Research*, 11, 1037–1045.
724 <https://doi.org/10.1093/plankt/11.5.1037>
- 725 Ryan-Keogh, T.R. & Smith, W.O., Jr. (2021). Temporal patterns of iron limitation in the Ross Sea
726 as determined from chlorophyll fluorescence. *Journal of Marine Systems*, 215,
727 <https://doi.org/10.1016/j.jmarsys.2020.103500>
- 728 Sætre, R. (1999). Features of the central Norwegian shelf circulation. *Continental Shelf Research*,
729 19, 1809-1831. [https://doi.org/https://doi.org/10.1016/S0278-4343\(99\)00041-2](https://doi.org/https://doi.org/10.1016/S0278-4343(99)00041-2)
- 730 Skagseth, Ø., Drinkwater, K.F., & Terrile, E. (2011). Wind- and buoyancy-induced transport of
731 the Norwegian Coastal Current in the Barents Sea. *Journal of Geophysical Research*, 116(C8),
732 <https://doi.org/10.1029/2011JC006996>
- 733 Søreide, J.E., Leu, E.V., Berge, J., Graeve, M., & Falk-Petersen, S. (2010). Timing of blooms,
734 algal food quality and *Calanus glacialis* reproduction and growth in a changing Arctic. *Global*
735 *Change Biology*, 16, 3154-3163.
- 736 Smith, W.O., Jr., & Asper, V. (2000). A balanced nitrogen budget of the surface layer of the
737 Southern Ross Sea, Antarctica. *Geophysical Research Letters*, 27, 2721-2724.
- 738 Smith, W.O., Jr., W.G. Zhang, W.G., Hirzel, A., Stanley, R.H.R., Meyer, M.G., Sosik, H.M., et
739 al. (2021). A regional, early spring bloom of *Phaeocystis pouchetii* on the New England
740 continental shelf. *Journal of Geophysical Research*, 126, e2020JC016856.
741 <https://doi.org/10.1029/2020JC016856>
- 742 Steemann Nielsen, E. (1952). The use of radioactive carbon (C14) for measuring organic
743 production in the sea. *Journal du Conseil International Exploration de Mer*, 18, 117–140.
744 <https://doi:10.1093/icesjms/18.2.117>

745 Wassmann, P., & Aadnesen, A. (1984). Hydrography, nutrients, suspended organic matter, and
746 primary production in a shallow fjord system on the west coast of Norway. *Sarsia*, 69, 139–
747 153.